Controlling frequency distance between individual modes of dielectric resonator nanoantenna using uniaxial anisotropic materials

# Controlling Frequency Distance between individual Modes of Dielectric Resonator Nano-antenna using Uniaxial Anisotropic Materials


| | |
|---|---|
| Journal: | *Photonics Journal* |
| Manuscript ID | PJ-011663-2021 |
| Manuscript Type: | Original Manuscript |
| Date Submitted by the Author: | 14-Mar-2021 |
| Complete List of Authors: | Fakhte, Saeed; Qom University of Technology,<br>Matekovits, Ladislau; Politecnico di Torino |
| Technical Area: Select one of the 12 Technical Areas that best describes the subject of your submission: your manuscript will be assigned to the corresponding Senior Editor: | Optical communications |
| Technical Topic: <b>Select one Technical Topic that best describes the subject of your manuscript</b>: | 22 Photonic materials and engineered photonic structures |
| Keywords: | Nano-antennas < Nanophotonics |
| | |

# Controlling Frequency Distance between individual Modes of Dielectric Resonator Nano-antenna using Uniaxial Anisotropic Materials

S. Fakhte and L. Matekovits

Saeed Fakhte (Qom *University of Technology, Qom, Iran*)
Ladislau Matekovits (*Department of Electronics and Telecommunications, Politecnico di Torino, 10129 Torino, Italy*)
E-mail: fakhte@qut.ac.ir

**Abstract: A technique to significantly shift down the resonant frequency of the higher order modes of an uniaxial anisotropic rectangular dielectric resonator nano-antenna (DRNA) without any considerable change in the resonant frequency of the fundamental mode is presented. The method aims to adjust the ratio of the resonant frequency of the higher order modes without changing the physical dimensions of DRA. This method can be used to adjust the frequency distance between the high-order and fundamental modes of the antenna. In this method, unlike the previously reported methods, it is possible to reduce the frequency distance between higher-order and fundamental modes of DRNA without the need for a very large height-to-length ratio. Due to the availability of naturally anisotropic dielectric materials in the optical band, such as TiO2, this design can be implemented in the optical band. The performances of the method are numerically validated for different contrast values between the dielectric tensor entries.**

***Index Terms*—Anisotropic, uniaxial, impedance bandwidth, dielectric resonator nanoantenna (DRNA).**

*Introduction:* Recently, much effort has been devoted to the exploration of dielectric resonator nano-antenna (DRNA) [1]-[3] due to great demand of highly efficient nano-antennas. In fact, at optical frequencies the electric field penetrates into the metal and couples with the surface plasmons, which results in high dissipation losses. But unlike metal-based antennas, the radiation mechanism in DRNA is derived from displacement currents, which leads to a higher radiation efficiency. The DRNA can be used for dual-band or multi-band applications [4]. For this purpose, multiple modes of the antenna at the desired frequencies should be excited. In the microwave regime, controlling the frequency distance between the individual modes of a dielectric resonator antenna (DRA) has been done by changing the ratio of height-to-length of the antenna [5]. By increasing the height-to-length ratio, the frequency distance between the fundamental and the high-order modes can be reduced. The disadvantage of this method is the large height-to-length ratio requirement for small frequency distance between the modes.

Recently, the use of anisotropic dielectric materials in DRAs has been investigated [6]-[7]. It has been reported that the use of these materials in DRA with proper design, improves antenna performances in terms of gain and in terms of bandwidth. One of the most widely used materials in optical band antennas, which also happens to be anisotropic, is $TiO_2$ [8]. The various unique applications of anisotropic DRNAs along with the availability of the natural anisotropic materials makes them a promising area which is yet to be explored.

In this paper, a new method for tuning the resonant frequency of the higher order modes of a rectangular DRNA is introduced. This is achieved by using a uniaxial anisotropic material, which optical axis corresponds to the normal of the rectangular prism faces.

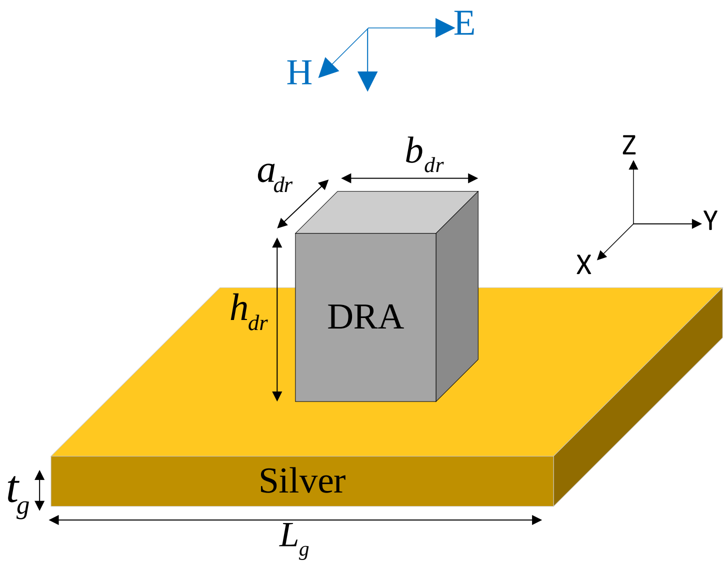


Fig. 1 The structure of proposed DRA.

*Antenna Configuration:* Fig. 1 shows the configuration of DRA mounted on a silver block with an area of $l_g \times l_g$ and a thickness of $t_g$. A plane wave excitation is used to excite the DRA. The dielectric resonator has dimensions $a_{dr}, b_{dr}, h_{dr}$ and permittivity dyadic of $\bar{\bar{\varepsilon}} = \varepsilon_o \bar{\bar{\varepsilon}}_r = \varepsilon_o(\varepsilon_x \bar{\bar{I}}_t + \varepsilon_z \hat{z}\hat{z})$, where $\bar{\bar{I}}_t$ is the transverse unit dyad with respect to $\hat{z}$ where $\hat{z}$ is the unit vector in the Z-direction. Since the penetration of the wave inside the metal in the optical band cannot be neglected, the Drude model has been used to describe the behaviour of the silver in this band. The silver permittivity is obtained by the following equation [9]:

$$\varepsilon_{Ag} = \varepsilon_\infty - \frac{\omega_p^2}{\omega(\omega + j\Gamma)} \qquad (1)$$

where $\varepsilon_\infty = 5$, the collision frequency $\Gamma = 1.12 \times 10^{14}\mathrm{Hz}$, and the plasma frequency $\omega_p = 2\pi \times 2.133 \times 10^{15}\mathrm{rad/s}$.

*Results and discussion:* Let consider a rectangular DRA filled with a uniaxial anisotropic media with the permittivity tensor elements of $\varepsilon_x$ and $\varepsilon_z$. The resonant frequency of the $TE^y_{mnp}$ mode can be obtained using different methods, as for example the dielectric waveguide model or the PMC cavity model [4]. Here, the PMC cavity model is used to obtain a straightforward relation between the resonant frequency and the ratio of elements of the permittivity tensor.

$$k_o^2 = \frac{1}{2\varepsilon_z}[k_x^2 + k_y^2 + R(k_y^2 + k_z^2) + \sqrt{\Delta}];$$
$$k_o = \frac{2\pi f_o}{c} \qquad (1)$$
$$R = \varepsilon_z / \varepsilon_x, k_x = \frac{m\pi}{a}, k_y = \frac{n\pi}{b}, k_z = \frac{p\pi}{d}$$

$$\Delta = k_x^4 + (1+R^2-2R)k_y^4 + R^2 k_z^4 + 2(1-R)k_x^2 k_y^2$$
$$+2(R^2-R)k_y^2 k_z^2 + 2Rk_x^2 k_z^2$$

where $c$ is the speed of light in free-space, $k_x$, $k_y$ and $k_z$ are the wave numbers inside the DRA and subscripts $m$, $n$ and $p$ represent the mode number indices in the x-, y- and z-directions, respectively. Also, $k_o$ is the free-space wave number.

Let's assume now that the value of $\varepsilon_z$ is very small with respect to that of $\varepsilon_x$, thus $R = \varepsilon_z/\varepsilon_x \approx 0$. Then from eq. (1) one gets:

$$k_0^2 \approx \frac{1}{\varepsilon_z}(k_x^2 + k_y^2). \quad (2)$$

Therefore, in this ideal case, the resonant frequency of $TE_{mnp}^y$ mode does not depend on $k_z$ and $\varepsilon_x$. For example, $TE_{11p}^y$(p=1, 2, …) modes will have the same resonant frequencies.

In practice, the ratio of $R = \varepsilon_z/\varepsilon_x$ is not equal to zero. So, the resonant frequency of the higher order modes can be close to that of the fundamental mode by choosing suitable values of $\varepsilon_x$ and $\varepsilon_z$ so that $\varepsilon_z/\varepsilon_x \ll 1$ is satisfied. In Table 1, the theoretical results of resonant frequencies for $TE_{111}^y$ and $TE_{113}^y$ modes ($f_1$ and $f_2$) of isotropic and anisotropic DRAs are presented, where the dimensions of DRAs and $\varepsilon_z$ are constant, but $\varepsilon_x$ varies. The theoretical results of the resonance frequency are obtained using the model reported by Fakhte et al [6]. Then, due to the penetration of the wave into the metal, the dimensions obtained through this method are multiplied by a scaling coefficient. The value of the scaling coefficient varies for the wavelength range of 0.5 to 10 µm [10], but in this work for simplicity the fixed value of 1.08 is considered, which happens to be in good agreement with the simulation results.

**Table I: Theoretical resonant frequencies of $TE_{111}^y$ ($f_1$) and $TE_{113}^y$ ($f_2$) modes of the anisotropic DRA, $l_x$=$l_y$=0.3 µm, $l_z$=0.375 µm.**

| Case | $\varepsilon_x$ | $\varepsilon_z$ | R | $f_1(Cal.)$ $[THz]$ | $f_2(Cal.)$ $[THz]$ | $\frac{f_2-f_1}{f_1}\%$ |
|---|---|---|---|---|---|---|
| A | 8 | 12 | 1.5 | 176 | 275 | 56.2 |
| B | 10 | 12 | 1.2 | 172 | 254 | 47.7 |
| C | 12 | 12 | 1 | 169 | 239 | 41.4 |
| D | 14 | 12 | 0.86 | 167 | 228 | 36.5 |
| E | 16 | 12 | 0.75 | 166 | 220 | 32.5 |
| F | 18 | 12 | 0.67 | 165 | 214 | 29.7 |
| G | 20 | 12 | 0.6 | 164 | 208 | 26.8 |
| H | 24 | 12 | 0.5 | 163 | 201 | 23.3 |

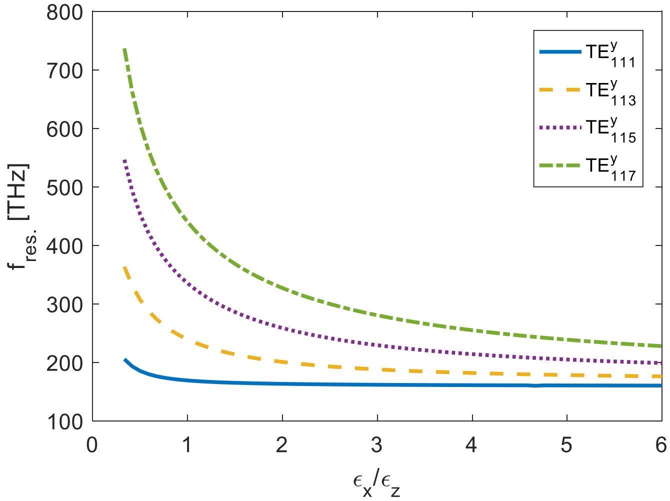


Fig. 2. Theoretical resonant frequencies versus $\varepsilon_x$ -to- $\varepsilon_z$ ratio for different modes of DRA. *a*=0.3 μm, *b*=0.3 μm, *d*=0.375 μm, $\varepsilon_z$=12.

Observe in Table 1 that by decreasing the value of the ratio $R = \varepsilon_z/\varepsilon_x$ from 1.5 to 0.5, the differences between the resonant frequencies of the higher order and fundamental modes are decreased from 56.2% to 23.3%. Also, as it can be observed in Fig. 2, by increasing the ratio of $\varepsilon_x$ -to- $\varepsilon_z$ (through decreasing R), the differences among the resonant frequencies of the $TE^y_{11p}$(p=1, 3, 5, 7) modes are drastically decreased. For example, the frequency separation between $TE^y_{111}$ and

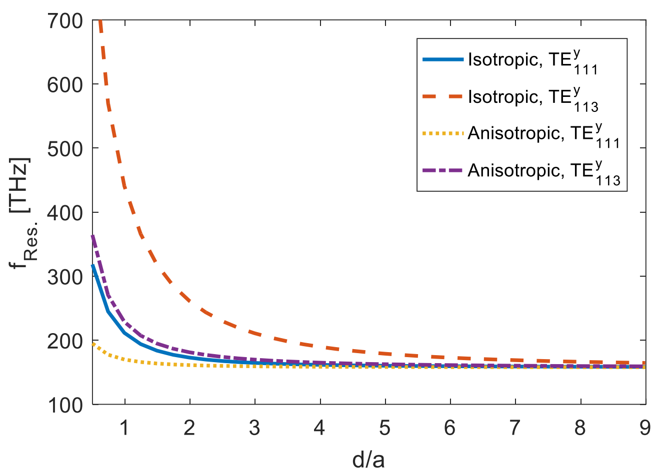


Fig. 3. Theoretical resonant frequencies versus height-to-length ratio for different modes of DRA. *a*=*b*=0.3 μm. For isotropic case: $\varepsilon_x = \varepsilon_z = 12$, and for anisotropic case: $\varepsilon_x = 72, \varepsilon_z = 12$.

$TE^y_{117}$ resonant modes is decreased from 271 THz for the isotropic case ($\varepsilon_x/\varepsilon_z = 1$) to the much smaller value of 68 THz for the anisotropic case ($\varepsilon_x/\varepsilon_z = 6$).

The variation of the resonant frequencies of the modes as a function of the height-to-length ratio for the isotropic ($\varepsilon_x = \varepsilon_z = 12$) and anisotropic ($\varepsilon_x = 72, \varepsilon_z = 12$) DRAs is also plotted in Fig. 3. Observe that the resonant frequency of the $TE^y_{111}$ mode of the isotropic DRA is independent from the height variations when the height-to-length ratio is larger than 3. This is because, by increasing the height-to-length ratio, the wave number in the z-direction (i.e., $k_z = \pi/d$) will be considerably smaller than those in the x- and y- directions, namely $k_x = \pi/a$ and $k_y = \pi/b$.

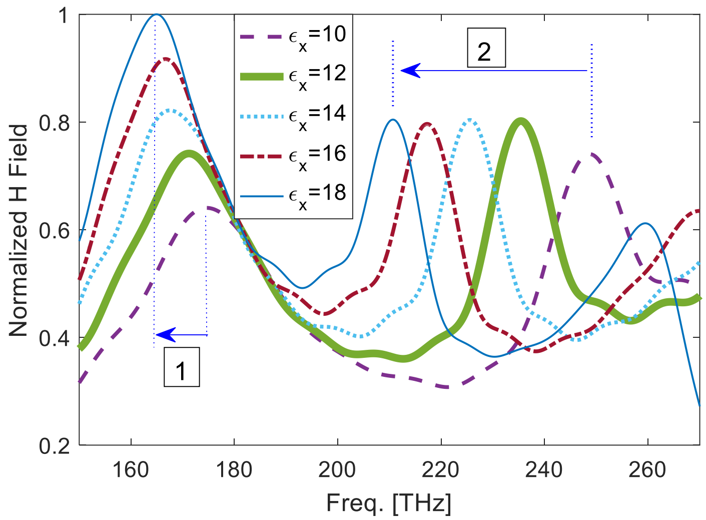


Fig. 4. Normalized magnitude of the magnetic field.

However, the resonant frequency of $TE_{113}^{y}$ mode for the isotropic DRA will not be sensitive to the height variation for the values of height-to-length ratio greater than 7, because of the larger values of wavenumber in the z-direction, namely $k_z = 3\pi/d$. By using the uniaxial anisotropic material with the permittivity ratio of $\varepsilon_x/\varepsilon_z = 6$, as it is proven, the resonant frequencies of both the $TE_{111}^{y}$and $TE_{113}^{y}$modes will not be sensitive to the height variations for the height-to-length ratios above 3. Consequently, by this method it will be possible to excite both the modes at nearly the same resonant frequency with much smaller height-to-length ratio compared to the isotropic case. The antennas mentioned in Table 1 are simulated and the results of these simulations are shown in Figure 4. The method of finding the resonant frequency of different DRA modes is such that a magnetic field probe is placed in the x direction below the DRA and in the middle of its lower surface. Then the magnitude of the normalized magnetic field is plotted in the frequency band of 150 to 270 THz. The frequencies corresponding to the peaks of this diagram indicate the resonance frequency of different antenna modes. For samples B to F listed in Table 1, simulations are performed. As shown in Figure 4, for each of these samples, two peaks are observed in the diagram, which correspond to the two DRA modes, so that the first and second peaks correspond to the $TE_{111}^{y}$ and $TE_{113}^{y}$ modes, respectively. It is observed that the simulated results of the resonance frequencies obtained from the simulation are close to the results of the theory mentioned in Table 1. Also, observe that the maximum frequency distance between the $TE_{111}^{y}$and $TE_{113}^{y}$modes is related to the anisotropic structure with $\varepsilon_x = 18$ and $\varepsilon_z = 12$. By increasing the ratio of $\varepsilon_x/\varepsilon_z$, the frequency distance between the fundamental mode and the high-order mode decreases, which confirms the results of the theory presented earlier. In Figure 4, arrow numbers 1 and 2 show the $TE_{113}^{y}$and $TE_{111}^{y}$ modes resonance frequency shifts by increasing the ratio of $\varepsilon_x/\varepsilon_z$. It is concluded that the resonant frequency of the higher order mode is drastically decreased while the one of the fundamental modes is not considerably changed.

For example, observe that for the isotropic DRA with $\varepsilon_x = \varepsilon_z = 12$, the $TE_{111}^{y}$and $TE_{113}^{y}$modes are excited at 171 THz and 235 THz, but for the anisotropic DRA the resonant frequencies of the $TE_{111}^{y}$and $TE_{113}^{y}$ modes are shifted down to 165 THz and 211 THz, respectively. The electric and magnetic field distributions of these modes which prove the excitation of the aforementioned modes are shown in Fig. 5. As it can be seen, the electromagnetic wave has penetrated into the

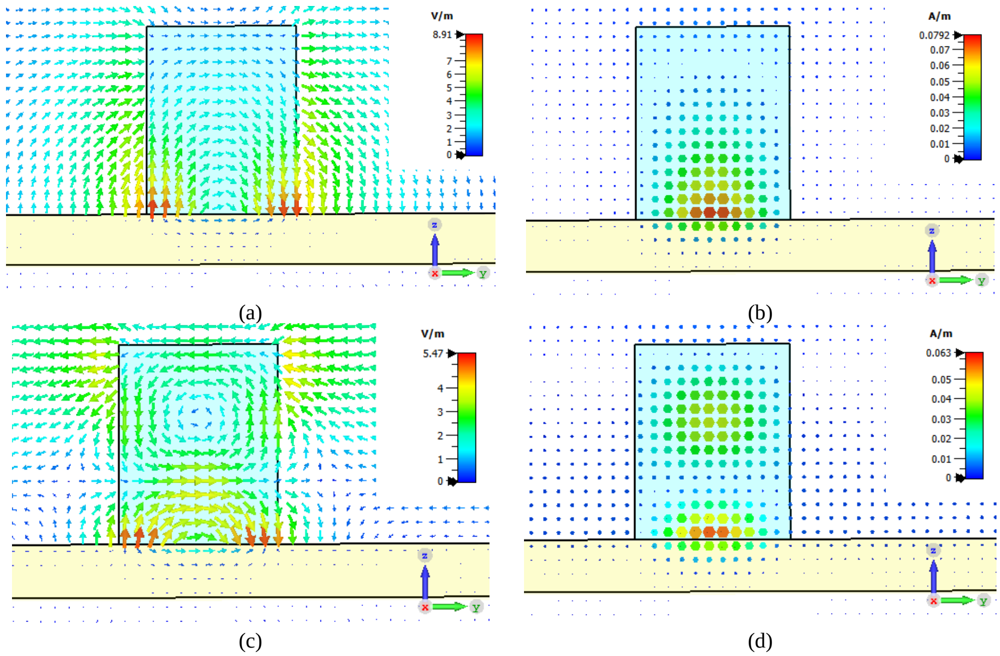


Fig. 5. Simulated field distribution of the anisotropic DRA (case F in Tab. I) at the plane x=0. (a) Electric field of $TE^{y}_{111}$ mode at 165 THz, (b) Magnetic field of $TE^{y}_{111}$ mode at 165 THz, (c) Electric field of $TE^{y}_{113}$ mode at 211 THz, (d) Magnetic field of $TE^{y}_{113}$ mode at 211 THz.

metal. In fact, by modelling the metal with the Drude model, the effect of wave penetration inside the metal on the antenna performance is also considered. As shown in Figs. 5(a) and (b), the electric and magnetic fields distributions resemble to the $TE^{y}_{111}$mode of the rectangular DRA. Also, the filed distributions in Figs. 5(c) and (d) resemble to $TE^{y}_{113}$ mode of the DRA. Therefore, it can be concluded that these two modes are properly excited.

Finally, note that the anisotropic tensors used in this work can be achieved using titanium dioxide ($TiO_2$). The refractive index matrix of $TiO_2$ is expressed by the following equation [8]:

$$n = \begin{pmatrix} n_x & 0 & 0 \\ 0 & n_y & 0 \\ 0 & 0 & n_z \end{pmatrix}$$
$$n_z^2 = 5.913 + 2.441\times10^7 / \left(\lambda^2 - 0.803\times10^7\right) \tag{3}$$
$$n_{x,y}^2 = 7.197 + 3.322\times10^7 / \left(\lambda^2 - 0.843\times10^7\right)$$

where $\lambda$ is in angstroms. One can obtain the permittivity tensor elements as follows: $\varepsilon_x = \sqrt{n_x}, \varepsilon_y = \sqrt{n_y}, \varepsilon_z = \sqrt{n_z}$. Figure 6 shows the permittivity tensor elements of the $TiO_2$ versus the wavelength. As can be seen, different $\varepsilon_x/\varepsilon_z$ ratios could be achieved across the wavelength.

*Conclusion:* A novel method for decreasing the frequency separation between the resonant modes of the DRNA is proposed. By using an uniaxial anisotropic material inside the DRNA prism, with

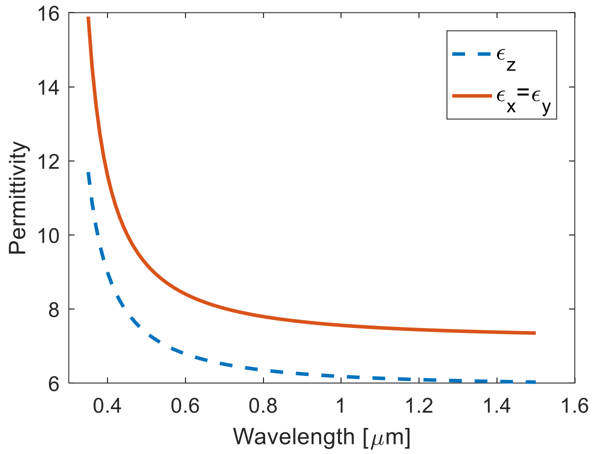


Fig. 6. Calculated permittivity tensor elements of the $TiO_2$.

proper design, the resonances of different modes can be adjusted to achieve a multiband response. Samples of simulation results are shown to demonstrate the capabilities of the proposed method for tuning the bands of operation.

**References**

1. G. N. Malheiros-Silveira and H. E. Hernandez-Figueroa, "Dielectric Resonator Nanoantenna Coupled to Metallic Coplanar Waveguide," in *IEEE Photonics Journal*, vol. 7, no. 1, pp. 1-7, Feb. 2015.
2. L. Zou et al., "Dielectric resonator nanoantennas at visible frequencies," Opt. Exp., vol. 21, no. 1, Jan. 2013, Art. ID. 1344.
3. L. Zou et al., "Efficiency and scalability of dielectric resonator antennas at optical frequencies," *IEEE Photon. J.*, vol. 6, no. 4, Aug. 2014.
4. Petosa, Dielectric Resonator Antenna Handbook, Norwood, MA, Artech House, 2007.
5. Rashidian and D. M. Klymyshyn, "Microstrip-fed high aspect ratio dielectric resonator antenna with dual-resonance broadband characteristics," in *Electronics Letters*, vol. 45, no. 2, pp. 94-95, Jan. 2009.
6. S. Fakhte, H. Oraizi and L. Matekovits, "High Gain Rectangular Dielectric Resonator Antenna Using Uniaxial Material at Fundamental Mode," in *IEEE Trans. on Antennas and Propagation*, vol. 65, no. 1, pp. 342-347, Jan. 2017.
7. S. Fakhte, H. Oraizi, L. Matekovits and G. Dassano, "Cylindrical Anisotropic Dielectric Resonator Antenna With Improved Gain," in *IEEE Trans. on Antennas and Propagation*, vol. 65, no. 3, pp. 1404-1409, March 2017.
8. E. D. Palik, Handbook of Optical Constants of Solids. New York, NY, USA: Academic, 1985.
9. S.-W. Qu and Z.-P. Nie, "Plasmonic nanopatch array for optical integrated circuit applications," *Scientific Reports*, vol. 3, no. 1, 2013.
10. L. Zou *et al*., "Efficiency and Scalability of Dielectric Resonator Antennas at Optical Frequencies," in *IEEE Photonics Journal*, vol. 6, no. 4, pp. 1-10, Aug. 2014.